A masking analysis of glass pattern perception

Chien-Chung Chen

Department of Psychology, National Taiwan University, Taipei, Taiwan, &
Neurobiology and Cognitive Science Center, National Taiwan University, Taipei, Taiwan

A Glass pattern consists of randomly distributed dot pairs (dipoles) whose orientations are determined by a geometric transform. To understand how an observer perceives the global structure, we investigated how the threshold for detecting a concentric or a radial Glass pattern (target) can be affected by the presence of another Glass pattern (masker). The Glass patterns had either concentric, radial, vertical, plaid, or spiral global forms. We used a 2AFC paradigm in which a mask was presented in both intervals while a target was randomly presented in one interval and a random dot pattern in the other. The target dot density thresholds were measured at 75% accuracy. For all masker types, the target threshold was constant at low masker densities and then increased with masker density. For concentric targets, concentric and spiral maskers had the best masking effect. For radial targets, a low-curvature spiral mask produced the best masking. The target threshold versus masker density functions were fit with a divisive inhibition model, in which the response of a global mechanism is the excitation of a linear template to the input image raised by a power and divided by the sum of an inhibition input and a constant.

Keywords: divisive inhibition, global shape, discrimination, noise, complex form

Citation: Chen, C.-C. (2009). A masking analysis of glass pattern perception. *Journal of Vision, 9*(12):22, 1–11, http://journalofvision.org/9/12/22/, doi:10.1167/9.12.22.

Introduction

A Glass pattern (Glass, 1969) is composed of randomly distributed dot pairs, or dipoles, whose relative orientation conforms to certain geometric rules that allow a normal observer to perceive the global structure in the pattern. It is suggested that at least two visual processes are involved in the human visual analysis of Glass patterns: the first is a local process which integrates neighboring dots into dipoles and the second is a global process which links dipoles to get the global structure (Cardinal & Kiper, 2003; Dakin & Bex, 2001; Mandelli & Kiper, 2005; Stevens, 1981; Wilson, Switkes, & De Valois, 2004; Wilson, Wilkinson, & Assad, 1997).

In the literature, it is suggested that the local and global processes can be separated by manipulating the various properties of Glass patterns. Studies focused on the local process manipulate the properties that may affect the ability of an observer to link dots into dipoles. Such manipulation can include changing the distance between the two dots in a dipole (Dakin, 1997; Kurki, Laurinen, Peromaa, & Saarinen, 2003) or allowing a difference in certain visual properties between the two dots, such as luminance contrast (Burr & Ross, 2006; Chen, 2006; Earle, 1999; Wilson et al., 2004), chromaticity (Mandelli & Kiper, 2005; Wilson & Switkes, 2005), spatial frequency (Dakin & Bex, 2001), or shape (Stevens, 1981). The researchers infer the properties of the local mechanisms by observing how these manipulations affect perception of the Glass pattern. On the other hand, to study the global process, one would need to manipulate the visual relationship between dipoles. For instance, Cardinal and Kiper (2003) measured how the visibility of a concentric Glass pattern of one chromaticity was affected when embedded in noise of another chromaticity.

While there have been studies on the tuning functions of the global pattern mechanisms (Webb, Roach, & Peirce, 2008), the response properties of these mechanisms are still poorly understood. Wilson and Wilkinson (1998, see also Wilson et al., 1997) proposed a multiple stage model for Glass pattern detection. Their model consists of two stages of linear filtering separated by a nonlinear process, with the first linear filters extracting the local information from a Glass pattern and the second extracting global information from the responses of the first filters. Their model, however, does not specify the response of the global mechanisms. In addition, their model focuses on the extraction of the global form from an image; it does not specify the interaction between two different global forms that may appear in the same image.

The purpose of this paper is to study the properties of the global process by observing how the visibility of the global structure in a Glass pattern (target) can be affected by the presence of another Glass pattern (masker). This kind of experimental paradigm, called "masking" in the literature, has been used widely to characterize the response nonlinearity (Chen & Tyler, 2001; Foley, 1994; Holmes & Meese, 2004; Kontsevich & Tyler, 1999; Legge & Foley, 1980; Ross & Speed, 1991) and tuning function (Chen & Tyler, 2002; Wilson, McFarlane, & Philips, 1983) of visual mechanisms. In the luminance contrast domain, it is known that the contrast threshold of a periodic target pattern changes with the visibility of the

doi: 10.1167/9.12.22 Received April 27, 2009; published November 30, 2009 ISSN 1534-7362

masker. If the masker is the same as the target in all spatiotemporal dimensions except contrast, the target threshold first decreases relative to the absolute threshold (facilitation) and then increases (masking) as the masker contrast increases (Chen & Tyler, 2001, 2008; Foley, 1994; Holmes & Meese, 2004; Kontsevich & Tyler, 1999; Legge & Foley, 1980; Ross & Speed, 1991). It is suggested that this "dipper"-shaped function of target threshold versus pedestal contrast (TvC) reflects the sigmoid-shaped contrast response functions of the target detection mechanisms (Chen & Tyler, 2001; Foley, 1994; Kontsevich & Tyler, 1999; Legge & Foley, 1980; Nachmias & Sanbury, 1974; Stromeyer & Klein, 1974). Furthermore, the shape of the TvC function for the same target may change with the composition and spatial properties of the masker (Chen & Foley, 2004; Foley, 1994; Holmes & Meese, 2004). This change in the TvC function shape may reflect the excitatory or inhibitory effect of the masker on the target detection mechanism (Foley, 1994). For instance, Chen and Foley (2004) showed that, for a concentric target, the dip of the TvC functions measured with a vertically oriented Gabor masker was shallower than that measured with a concentric masker. This shallower dip suggests that a vertical masker produces a weaker excitatory effect than a concentric one in the concentric pattern detector.

We adopted this masking paradigm for the study of global form mechanisms in the visual system. Following the paradigm of Chen and Foley (2004), we measured target threshold with the presence of maskers with various global forms and intensity. By comparing how the target threshold changes with masker intensity for different masker types, it is possible to reveal the interactions between global forms in determining the response properties of the target detection mechanism.

It is known that the detectability of a Glass pattern embedded in noise decreases with the density of the noise pattern (Maloney, Mitchison, & Barlow, 1987). Such noise-masking paradigm is useful to estimate the coding efficiency of the detection mechanisms. However, since noise is a broadband stimulus that may affect a wide range of mechanisms, it is not suitable to pinpoint the tuning properties of a particular global form detector. In addition, such a broadband stimulus may produce less effect in a particular detector than a stimulus whose global form matches the preferred form of that detector. Hence, a noise stimulus may not be able to produce a sufficiently strong response in the detection mechanism that allows us to estimate the response properties of the detection mechanism in the high response range. Thus, for our purpose, noise masker alone is not sufficient.

The current theories for estimating nonlinear properties of the visual mechanisms from masking experiments were developed primarily for periodic patterns. To apply them to masking experiments with Glass patterns, we first need to deal with two issues. The first is the measurement of visibility. The most common measurement of the visibility of a Glass pattern is coherence threshold (Wilson & Wilkinson, 1998; Wilson et al., 2004). A lower coherence threshold means that the observer can perceive the global structure with fewer signal dipoles (i.e., pairs whose orientation conforms to the predesignated mathematic transforms) amid a larger number of noise dipoles. Hence, it is easier to detect the global structure of a Glass pattern with a lower coherence threshold than one with a higher coherence threshold. This measurement has a serious problem when applied to a masking experiment. When one superimposes the target on the masker, the noise dipoles of the two patterns mix together. As a result, it is impossible to determine the coherence of either the target or the masker. For instance, suppose that the target has m_1 signal dipoles and m_2 noise dipoles while the masker contains n_1 signal dipoles and n_2 noise dipoles. That is, the target has a coherence $m_1 / (m_1 + m_2)$. When superimposed, the signal-plus-masker pattern contains $m_2 + n_2$ noise dipoles. This pattern can be taken as either a target of 1.0 coherence on a masker of $n_2 / (m_2 + n_2)$ coherence or a target of $n_1 / (m_2 + n_2)$ coherence on a masker of 1.0 coherence, or anything in between. There are other measurements of visibility in the literature, such as the maximum distance between dots in a dipole (Dakin, 1997; Kurki et al., 2003) or the maximum jitter of the orientation of the signal dipoles (Dakin, 1997). The former, however, may confound local and global processing, while the latter may create a new global structure different from that of the target (for instance, an orientation jitter of signal dipoles in a concentric pattern may result in a sum of two spiral patterns: one clockwise and the other counterclockwise). The second issue is that when a target is superimposed on a masker, the total number of dipoles is greater than that of the masker alone. Hence, an observer may simply use this difference in image statistics rather than perceived global structure to make responses.

To solve these two problems, our strategy utilizes the phenomenon that the human ability to perceive the global structure improves with the number of dipoles (Maloney et al., 1987). Hence, the target threshold was measured as the number of dipoles required for an observer to discern a target Glass pattern from a control pattern that consisted of only noise dipoles in the same number. The intensity of the masker was then controlled by manipulating the number of signal dipoles in the Glass pattern without the presence of noise dipoles. This paradigm also has another advantage, as it kept the total number of dipoles the same in both intervals of a two-alternative forced-choice trial.

Method

Apparatus

The stimuli were presented on two Viewsonic 15-in. monitors, each driven by a Radeon 7200 graphic board

that provided 10-bit digital-to-analog converter depth. A Macintosh computer controlled the graphic boards. Lights from the two monitors were combined by a beam splitter. This two-monitor setup allowed us to present the target on one monitor and the masker on the other. This arrangement gave us the advantage of independent control of the target and the masker. The viewing field was 13.3° (H) × 10° (V). The resolution of the monitors was 800 horizontal × 600 vertical pixels, giving 60 pixels per degree at the viewing distance used (128 cm). The refresh rate of the monitor was 66 Hz. We used the LightMouse photometer (Tyler & McBride, 1997) to measure the full-detailed input–output intensity function of the monitor. This information allowed us to compute linear lookup table settings to linearize the output within 0.2%. The maximum luminance of the display was set at 90 cd/m^2.

Stimuli

A Glass pattern consisted of pairs of 1′ × 1′ random dots. The size of the image was 10° × 10° or 600 × 600 pixels. The number of dipoles was determined by d (the product of the density parameter) and half the number of pixels. The position of half of the dots, that is, the first dot in each dipole, was generated with a random number generator and distributed evenly in space. The position of the second dot in a dipole was determined by the position of the first dot and the desired global structure.

Figure 1A shows examples of our stimuli. The target was either a concentric or a radial pattern. There were seven types of maskers: concentric, radial, vertical, plaid, noise, and two types of spiral. The noise pattern was simply a zero coherence Glass pattern. That is, while the distance between two dots in a dipole was fixed as in the other patterns, the orientation of the dipoles was randomized. The contours of the other types of Glass patterns were defined by the following equations:

$$\begin{aligned} x &= k(\text{vertical}) \\ y &= k(\text{horizontal, used in plaid pattern}) \\ r &= k(\text{concentric}) \\ \theta &= k(\text{radial}), \end{aligned} \tag{1}$$

and

$$r = k + b\theta(\text{spiral}), \tag{2}$$

where k was a constant depending on the position of the first dot, $r = (x^2 + y^2)$, $\theta = \tan^{-1}(y / x)$. The second dot in a dipole was placed such that the orientation of the dipoles was tangent to the contour, and the distance between the two dots in a dipole was always 5′. The parameter b controlled the curvature of the spiral. We used spiral patterns of two curvatures: the high-curvature pattern, called Spiral 1, had $b = 0.16$ and the low curvature one, Spiral 2, $b = 1.6$, when the unit of θ was radiance of arc length while the unit of r was radiance of visual angle. The plaid pattern consisted of a combined vertical and horizontal pattern, each containing half the number of the total dipoles in the pattern.

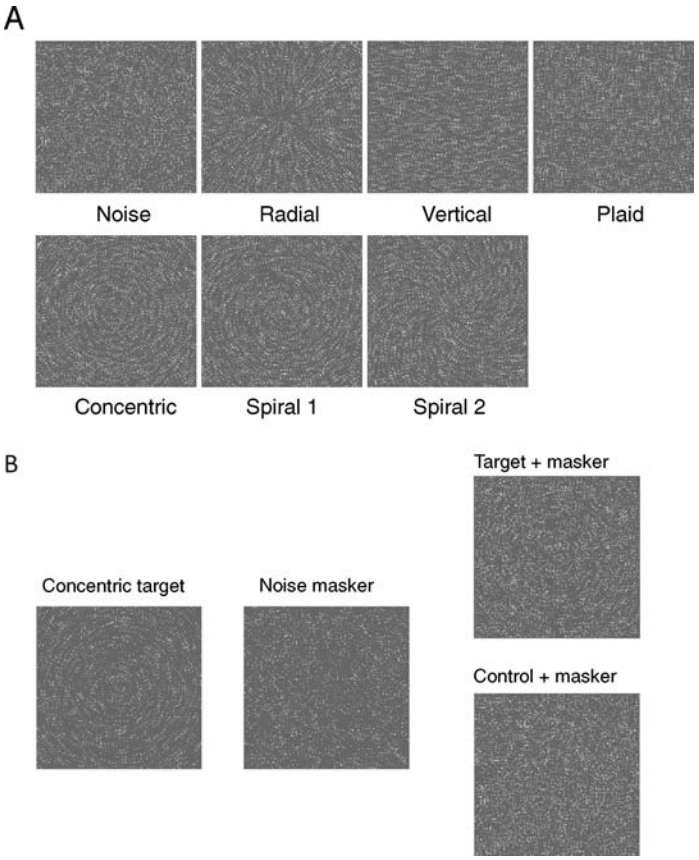

Figure 1. (A) Examples of seven types of Glass patterns used in the experiment. (B) Examples of a concentric target (left), a noise masker (middle), and the stimuli in both target (right, top) and control (right, bottom) intervals in a 2AFC trial.

Procedure

A two-alternative forced choice (2AFC) paradigm and a PSI (Kontsevich & Tyler, 1999) adaptive threshold-seeking algorithm were used to measure the threshold at 75% correct response level. The masker was presented in both intervals. The target stimulus was randomly presented with equal probability in either of the two intervals, while a pattern with randomly oriented dipoles of the same density was presented in the other interval. Figure 1B shows examples of the stimuli in both intervals. The duration of each interval was 300 ms. The task of the observer was to determine which interval contained the target. Each threshold measurement contained 40 2AFC trials.

There were three observers (one male and two female) involved in this study. All observers had corrected to

normal (20/20) visual acuity. One observer was the author of this paper and two others were paid observers who were naïve as to the purpose of the experiment.

Results and discussion

TvD functions

Figure 2 shows the target threshold versus masker density (TvD) functions for detecting the concentric target Glass pattern. Each data point was an average of 4–8 threshold measurements of the same condition. The error bar represents the standard error of the measurements. For the noise masker (closed circles and solid curves), the target threshold was flat at low masker density to a certain critical value and then increased with masker density. Such behavior is very similar to the detection of a luminance-modulated pattern on a noise pedestal (Legge, Kersten, & Burgess, 1987; Lu & Dosher, 1998). The smooth curves in this and the subsequent figures are the fits of the divisive inhibition model discussed later in the paper.

The magenta upper triangles and dotted curves in Figure 2 denote the TvD functions for the vertically oriented masker; the red lower triangle and dash-dotted curves, the plaid masker; and the green open squares and dashed curves, the radial masker. The TvD functions for these maskers with oriented global structure were all very similar to those for the noise masker. Neither maskers showed any facilitation effect on concentric Glass pattern detection. In fact, all showed a masking effect.

Figure 3 shows TvD functions for detection of the concentric target on curved maskers. The green closed squares and dashed curves denote the TvD functions for the concentric masker; the magenta open upper triangles and dotted curves, the spiral masker with high curvature (Spiral 1); and the red closed lower triangle and dash-dotted curves, the spiral masker with low curvature (Spiral 2). In general, the maskers with curved global structure produced a greater masking effect than oriented maskers did. Figure 4 illustrates this. In this figure, we plot the threshold elevation produced by various maskers at the same masker density of 0.1. The maskers without curved global structure produced a threshold elevation of 0.4 to 0.7 log units while those with curved global structure had an elevation of 0.7 to 1.7 log units across different observers and maskers. In addition, with the exception of the plain masker, there was little, if any, difference between the threshold elevation produced by the noise masker (horizontal dashed lines in Figure 4) and that produced by maskers with oriented global structure. On the other hand, maskers with curved global structure always showed significantly greater masking effects (denoted by asterisk symbols in Figure 4) than the noise masker.

We also observed individual differences in the TvD functions for curved maskers. One observer (CC) showed

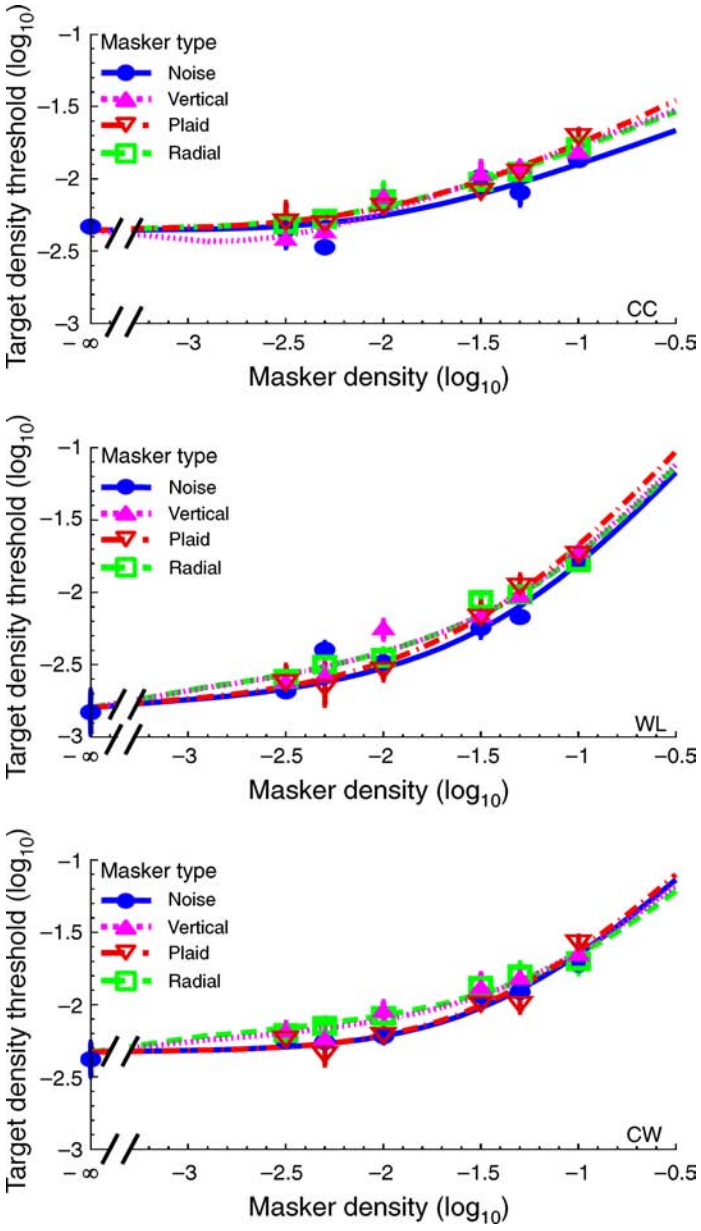

Figure 2. The TvD functions for the concentric target on the noise and oriented maskers. Each panel contains data from one observer. The error bar represents one standard error of measurement. Blue closed circles and solid curves: noise masker. Magenta upper triangles and the dotted curves: vertically oriented masker. Red lower triangle and the dash-dotted curves: plaid masker. Green open squares and the dashed curves: radial masker.

dipper shape TvD functions with a facilitation effect at low masker density for the two spiral maskers, while the other two observers only showed the masking effect at high masker densities. Nevertheless, this difference can be accounted for by the same model (discussed below) as shown by the smooth curves in Figures 3 and 4.

Figure 5 shows the TvD functions for detection of the radial target on oriented maskers. The masker type represented by each symbol in this figure is the same as

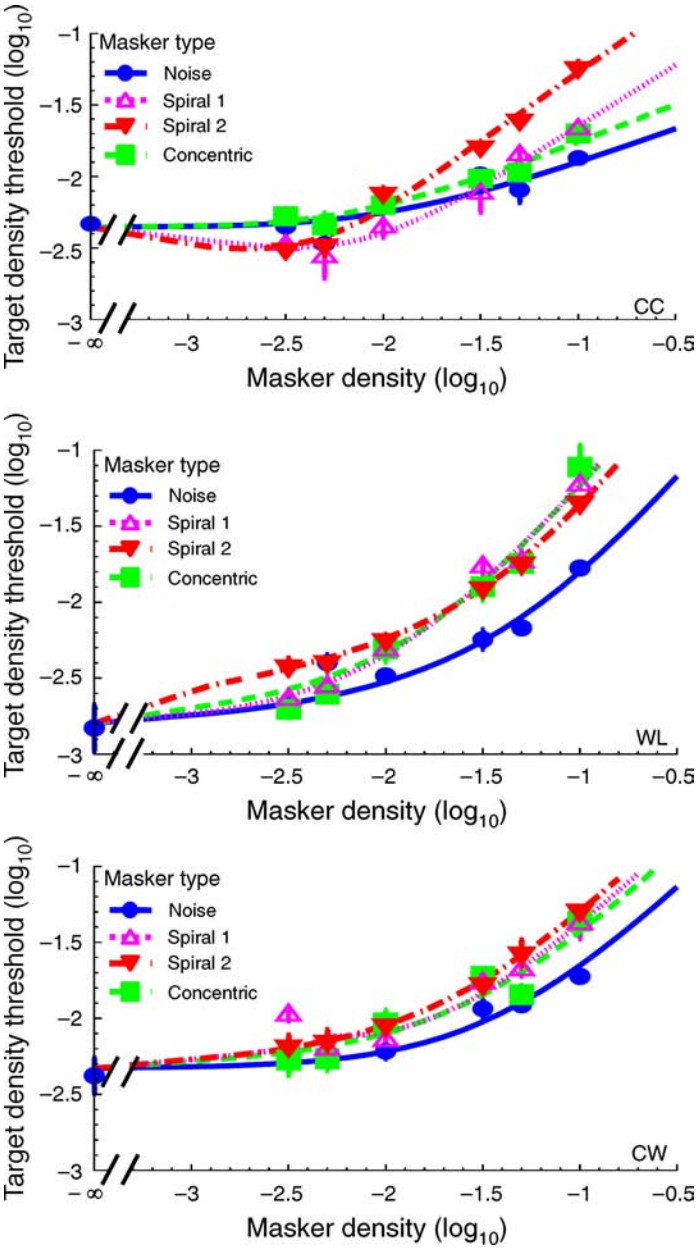

Figure 3. The TvD functions for the concentric target on curved maskers. The TvD functions for the noise masker (blue closed circles and solid curves) are re-plotted here for comparison. The error bar represents one standard error of measurement. Green closed squares and dashed curves: concentric masker. Magenta open upper triangles and dotted curves: Spiral 1. Red closed lower triangles and dash-dotted curves: Spiral 2.

that in Figure 2. For all observers, the threshold was higher for the radial target than for the concentric pattern. On average, this difference was 0.41 log unit or 2.6-fold. This suggests that the visual system may be less sensitive to a radial target then a concentric one. The shapes of the TvD functions were quite similar to those for the concentric target. For the noise masker, the target threshold was flat at low masker density up to a certain critical value and then increased with masker density. The TvD functions for other oriented maskers were all very similar to those for the noise masker. All TvD functions overlapped with each other, with the only exception being the vertical and plaid masker functions for observer CW, which showed a greater masking effect at medium densities. Again, as the smooth curves show, such individual differences can be accounted for by the same model discussed below. Notice that the TvD function for the radial masker was not very different from those for the other maskers even though, in this condition, the target and the masker had the same global form.

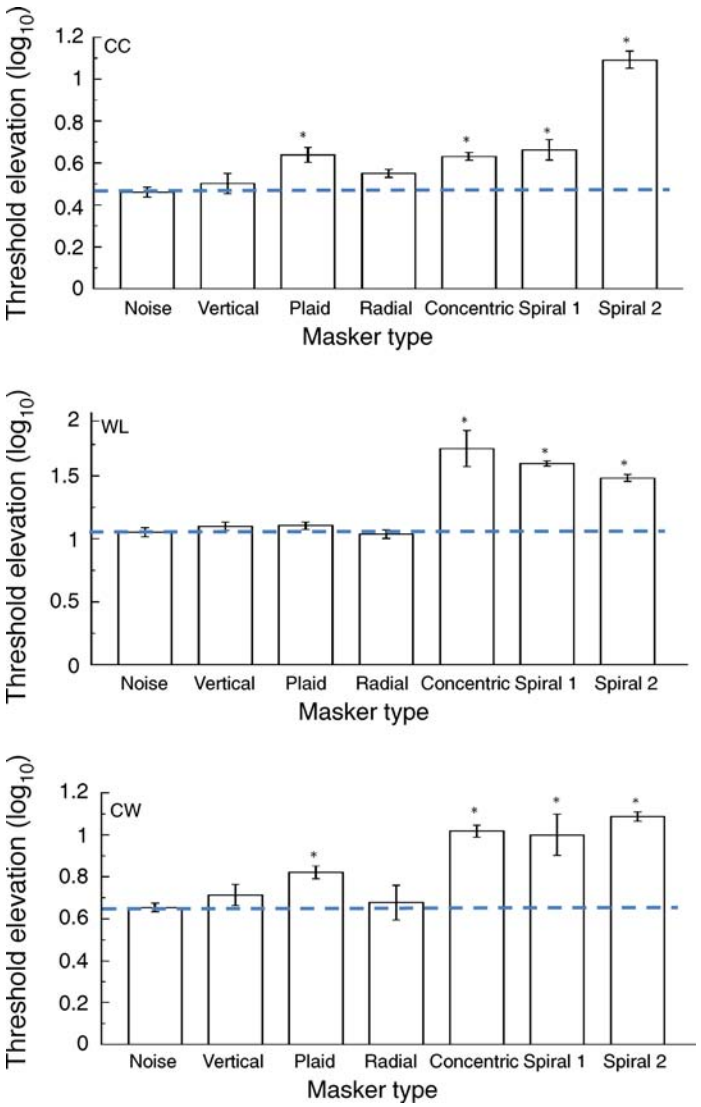

Figure 4. Threshold elevation of the concentric target produced by different masker types at 10% (−1 log unit) masker dot density. The error bar represents one standard error of measurement. For comparison, the horizontal dashed line denotes the threshold elevation produced by the noise masker. The "*" above a bar denotes a statistically significant difference in threshold elevation produced by that type of the masker and the noise masker.

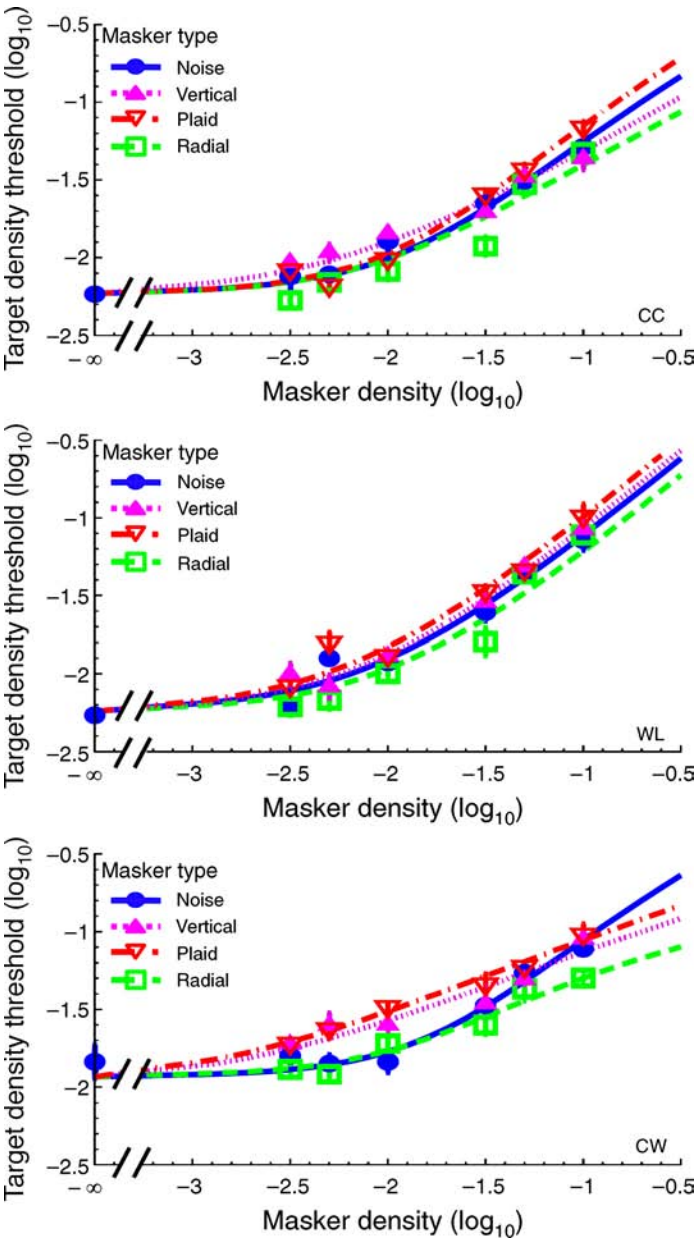

Figure 5. The TvD functions for the radial target on the noise and oriented maskers. Each panel contains data from one observer. The error bar represents one standard error of measurement. Blue closed circles and solid curves: noise masker. Magenta upper triangles and the dotted curves: vertically oriented masker. Red lower triangle and the dash-dotted curves: plaid masker. Green open squares and the dashed curves: radial masker.

Figure 6 shows the TvD functions for detection of the radial target on curved maskers. The masker type represented by each symbol is the same as in Figure 3. Overall, the result was similar to the TvD functions for the concentric target except that the low-curvature spiral masker (Spiral 2) had a distinct advantage in producing the masking effect. The masker-dependent threshold elevation is illustrated in Figure 7. In this figure, we plot the threshold elevation produced by various maskers at the same masker density of 0.1. The low-curvature spiral masker (Spiral 2) produced a masking effect that, across different observers, was 0.32–0.43 log unit or 2.1–2.7 times more than that produced by the noise masker and 0.40–0.5 log unit or 2.5–3.2 times more than that produced by the radial mask itself. Such strong "field sensitivity" (Stiles, 1959) suggests that the radial pattern detector is

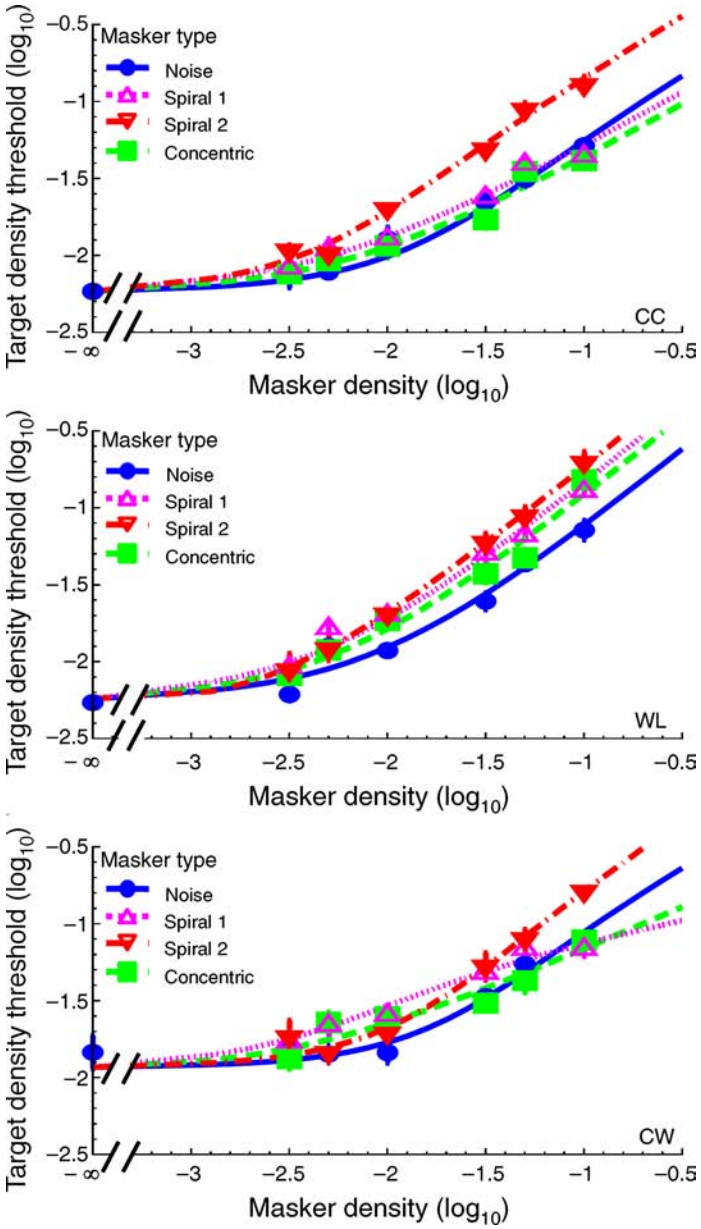

Figure 6. The TvD functions for the radial target on the curved maskers. The TvD functions for the noise masker (blue closed circles and solid curves) are re-plotted here for comparison. The error bar represents one standard error of measurement. Green closed squares and dashed curves: concentric masker. Magenta open upper triangles and dotted curves: Spiral 1. Red closed lower triangles and dash-dotted curves: Spiral 2.

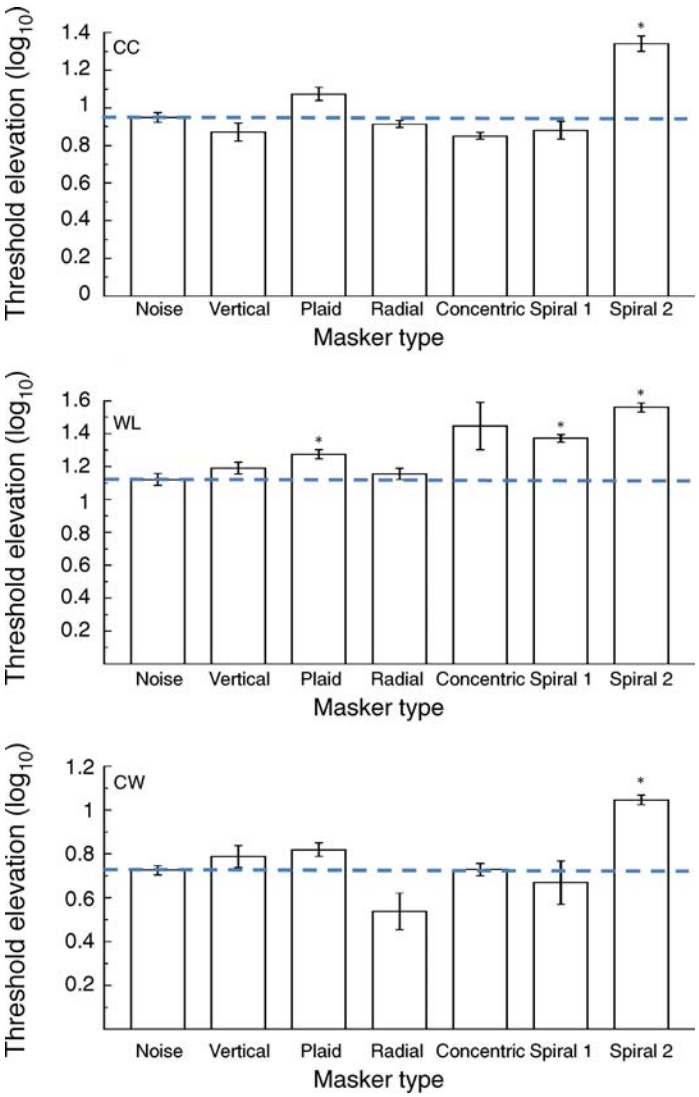

Figure 7. Threshold elevation of the radial target produced by different masker types at 10% (−1 log unit) masker dot density. The error bar represents one standard error of measurement. For comparison, the horizontal dashed line denotes the threshold elevation produced by the noise masker. The "*" above a bar denotes a statistically significant difference in threshold elevation produced by that type of the masker and the noise masker.

more sensitive to a low-curvature spiral pattern than to the radial pattern itself.

Model

It has been suggested that the processing of Glass patterns involves both local and global processing. The local processing involves oriented linear filters that extract dipole information, followed by a nonlinear operation, such as rectification. The global processing therefore operates on the output of local processing (Wilson & Wilkinson, 1998). In this study, we did not manipulate the properties of individual dipoles that might affect the response of the local linear filters. Hence, without losing generality, we may assume that each dipole produces the same responses in a local filter whose orientation and location tuning matches those of the dipole. Thus, in this study, we only need to consider the mechanisms of the global processing which receives the contribution of the local filters.

Figure 8 illustrates our model of the global Glass pattern mechanism. This model shares many features with pattern vision models that have successfully accounted for a wide range of pattern discrimination data (Chen, Chen, Tseng, & Kuo, 2009; Chen & Foley, 2004; Chen, Foley, & Brainard, 2000; Foley, 1994). The global mechanism contains several stages. The first stage involves a linear template (or the second-order filter in Wilson & Wilkinson, 1998) that integrates dipoles whose orientation is consistent with the preferred shape of the template. The other dipoles exert their influence as a divisive inhibition input from other mechanisms. The response of the mechanism is the excitation of the linear template raised by a power and then divided by the sum of the divisive inhibition input plus an additive constant.

It is reasonable to assume that the detection threshold may be dominated by a mechanism that has the greatest difference in response between the target and the noise pattern. Thus, we can assume that the linear template has a sensitivity profile close to that of the target. Such an assumption is reasonable because there are neurons in the area V4 whose receptive fields have either a concentric or a radial structure (Gallant, Braun, & Van Essen, 1993), and it has been suggested that these types of neuron may be responsible for Glass pattern detection (Wilson & Wilkinson, 1998).

Let h be the response of each local dipole filter to a dipole. Hence, the contribution of kth dipole to a jth linear template in the ith image would be $a_{i,jk} \times h$, where $a_{i,jk}$ is a weighting constant. The value of the weighting constant

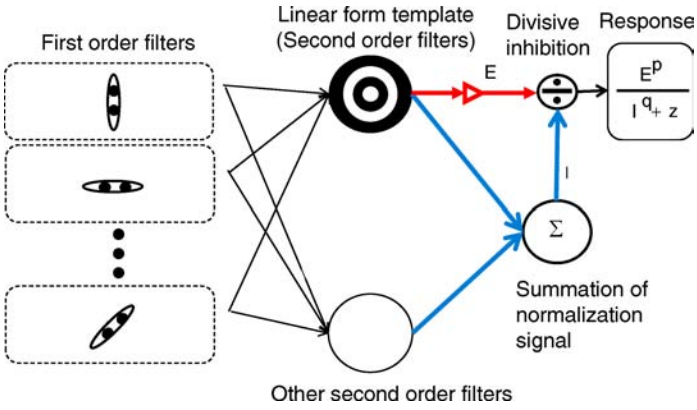

Figure 8. Diagram of the divisive inhibition model that fits the masking data. Notice that while the sensitivity profile of the second-order filter shown here has a concentric structure, it can be replaced by another filter with different global structure. See text for detail.

$a_{i,jk}$ will be greater if the orientation of the kth dipole is consistent with the sensitivity profile of the jth linear template and smaller if not. Integrating all local filters, the excitation of the jth linear template to ith pattern, E_{ij}, is

$$E_{ij} = \sum_{k=1}^{n} (a_{i,jk} \times h), \tag{3}$$

where n is the number of dipoles in the image. That is, the excitation of the global linear template is a linear combination of the contribution of individual dipoles. The magnitude of excitation depends on both the number of dipoles in the image (n) and the correspondence between the image and the template that determines the value and the distribution of $a_{i,jk}$. Thus, the excitation can be rewritten as

$$E_{ij} = \mathrm{Se}'_{ij} \times n, \tag{3'}$$

where $\mathrm{Se}' = \sum_{k=1}^{n} (a_{i,jk} \times h) / n$.

For a better comparison with previous results in the literature, we multiply the number of dipoles by two to get the number of dots in a Glass pattern and then scale it with the total number of pixels in the display to get the dot density of the Glass pattern, d. Hence, Equation 3′ becomes

$$E_{ij} = \mathrm{Se}_{ij} \times d, \tag{4}$$

where Se_{ij} is Se'_{ij} times the number of possible dots in the image. Se_{ij} thus controls the contribution of the ith pattern to the jth template in our model. We constrained Se_{ij} to be positive for all conditions.

While we derived Equation 4 from the agreement between the dipole orientations and a global template, this equation can be derived from the filter model for Glass patterns (Wilson & Wilkinson, 1998) as well. For the sparse random dot patterns we used, each additional dipole increases the contrast energy in the image by a constant amount. Hence, the response of a linear filter should increase proportional to the dot density.

Notice that, in our data, the target threshold increased with masker density regardless of the masker type. Such threshold increment suggests a deceleration in the response function (Chen & Tyler, 2001; Foley, 1994; Legge & Foley, 1980; Nachmias & Sansbury, 1974). That is, the response increases less for the same increment in number of dipoles. Such deceleration can be achieved by providing a divisive input to the response function (Foley, 1994). Thus, the response of the global mechanism is the excitation raised to a power p and divide by the sum of a divisive inhibition term, I, and an additive constant, z. That is,

$$R_j = E_j^p / (I_j + z). \tag{5}$$

The divisive inhibition input is a nonlinear combination of the rectified excitations of all relevant mechanisms, that is, those which have non-zero response to the stimuli, given by

$$\begin{aligned} I_j &= \sum\nolimits_m w_m E_n^q \\ &= \mathrm{Si}_j \cdot C^q, \end{aligned} \tag{6}$$

where $\mathrm{Si}_j = \sum_m (w_m \mathrm{Se}_j^q)$ is the sensitivity of the jth mechanism to the divisive inhibition input.

In our two-interval forced choice experiment, the difference in response is given as

$$D = R_{j,b+t} - R_{j,b+n}, \tag{7}$$

where j is the mechanism that gives the greatest response difference, and $b + t$ denotes the pattern in the target-plus-masker interval, while $b + n$ denotes the pattern in the noise-plus-masker interval. The target reaches the threshold when D reaches a certain amount (Legge & Foley, 1980), designated as 1 in our model fitting.

The fits of the model were shown as smooth curves in Figures 2, 3, 5, and 6. The model fit the data quite well. Across three observers, this model accounted for 95.6–96.9% of total variability in the data. The rooted mean square errors (RMSE) of the fits were 0.052 to 0.072 across observers and target conditions, while the range of standard error was 0.045 to 0.060 log units. The parameter values are shown in Table 1. Notice that the excitatory sensitivity to the concentric pattern was fixed at 100.

	Observers		
Parameters	CC	CW	WL
p	1.55	1.30	1.06
q	1.09	1.00[a]	1.00[a]
z	0.11	0.19	0.07
Se			
Concentric	100[a]	100[a]	100[a]
Spiral 1	74.84	97.63	130.68
Spiral 2	100.92	109.01	55.21
Vertical	29.05	16.40	1.96
Plaid	28.33	34.45	65.88
Radial	25.38	19.09	3.04
Noise	27.95	36.70	57.69
Si			
Concentric	32.30	17.08	3.71
Spiral 1	14.16	14.23	5.07
Spiral 2	23.03	23.17	14.78
Vertical	26.19	16.66	6.87
Plaid	28.21	3.48	3.33
Radial	26.07	17.75	6.80
Noise	22.54	6.81	2.27

Table 1. Fitted model parameters for the concentric target. *Note*: [a]Fixed number, not a free parameter.

Parameters	Observers		
	CC	CW	WL
p	1.23	0.98	1.71
q	0.97	1.00[a]	1.00[a]
z	0.12	0.07	0.09
Se			
Concentric	81.88	250.46	0.38
Spiral 1	69.64	56.71	370.21
Spiral 2	225.49	1589.89	126.82
Vertical	48.41	35.34	54.37
Plaid	92.65	35.88	57.22
Radial	100[a]	100[a]	100[a]
Noise	63.07	83.43	82.35
Si			
Concentric	15.40	20.31	3.71
Spiral 1	25.26	16.70	36.64
Spiral 2	18.66	54.75	10.57
Vertical	23.58	9.30	113.90
Plaid	7.30	9.30	151.82
Radial	9.69	9.30	9.66
Noise	6.34	10.51	7.05

Table 2. Fitted model parameters for the radial target. *Note*: [a]Fixed number, not a free parameter.

The power for the divisive inhibition input was very close to one. This is quite different from its counterpart in the contrast pattern studies, which tended to be around 2 to 2.4 (Foley, 1994). Indeed, two observers showed no significant sum of squared error (SSE) increment ($F(2,53) = 1.03$, $p = 0.36$ for CW and $F(2,53) = 097$, $p = 0.39$ for WL) by fixing $q = 1$. The parameter values in Tables 1 and 2 and fitted curves in Figures 2, 3, 5, and 6 reflect this constraint.

Shape tuning

The shape of TvD functions changes with masker type for concentric patterns, as shown above. This implies a shape tuning in the global form detector. The TvD functions for the vertical and radial maskers were similar to that of the noise masker. The plaid masker created significantly greater threshold elevation than the vertical masker (Figures 2 and 4). The value of the model parameters suggests that this effect may be due to a greater sensitivity of the linear template to the plaid (Table 1). The plaid masker we used was just a combined vertical and horizontal pattern with half dot density. Thus, a plaid should produce the same activation as a vertical pattern of the same dot density in a linear template with concentric structure. This effect may suggest an intermediate stage that sums dipoles of different orientations into local curved fragments. A plaid contains many vertical and horizontal dipoles that are placed near each other and thus could be considered as two different parts of an arc. Hence, a plaid should produce more activation than a vertical pattern in a local curve detector and, in turn, in a concentric pattern detector.

All curved maskers produced significant masking effects for concentric targets at high dot density (Figures 3 and 4). Model parameters also showed that the target mechanism has a greater sensitivity to these patterns. Even the radial pattern detector showed a preference for curved patterns: the masker that showed the greatest masking effect was not the radial pattern itself but the low-curvature spiral (Figures 6 and 7). In addition, the concentric pattern and the high-curvature spiral pattern also had less effect than the low-curvature spiral. Note that the low-curvature spiral looks more similar to the radial pattern than the other maskers. Hence, the radial pattern detector also showed a shape tuning. It is just that the best tuned shape was closer to the low-curvature spiral than the radial pattern itself.

This result is consistent with previous findings that Glass pattern detectors prefer curved patterns over oriented ones (Wilson et al., 1997). The amount of threshold elevation and the value of sensitivity parameters changed with the curvature of the masker. This implies a curvature-dependent response in the target detector. Webb et al. (2008) measured the threshold increment for detecting spiral texture patterns in the presence of other spiral texture patterns. Seu and Ferrera (2001) measured spiral Glass pattern in the presence of noise. They also reported a curvature-dependent threshold elevation. Clifford and Weston (2005) also reported a shape tuning for Glass patterns with an adaptation paradigm.

Signal-to-noise ratio analysis

In the noise mask condition, the task of the observer was to detect a signal pattern (i.e., a target) at different noise levels. This task was similar to the external noise paradigm (Legge et al., 1987; Lu & Dosher, 1998, 2008; Pelli, 1990) that has been used to characterize the limitation and efficiency of the visual mechanisms. In particular, this condition is similar to the experiment reported by Maloney et al. (1987) who measured the discriminability of Glass patterns in the presence of noise maskers with different number of dots. They showed that discriminability (d') increased with the number of dipoles in the target and decreased with the number of dots in the noise masker and that d' could be explained by a function of the signal to noise ratio in the image. Their signal-to-noise ratio analysis implies that the threshold (i.e., the number of signal dots at a certain d' level) is proportional to the number of noise dots. This implies that the TvD function should have a fixed slope. This result, however, cannot be generalized to the various masking conditions we measured. The slope of TvD functions depends on both the target and the masker. As shown in Figure 9, the slope varied for different maskers.

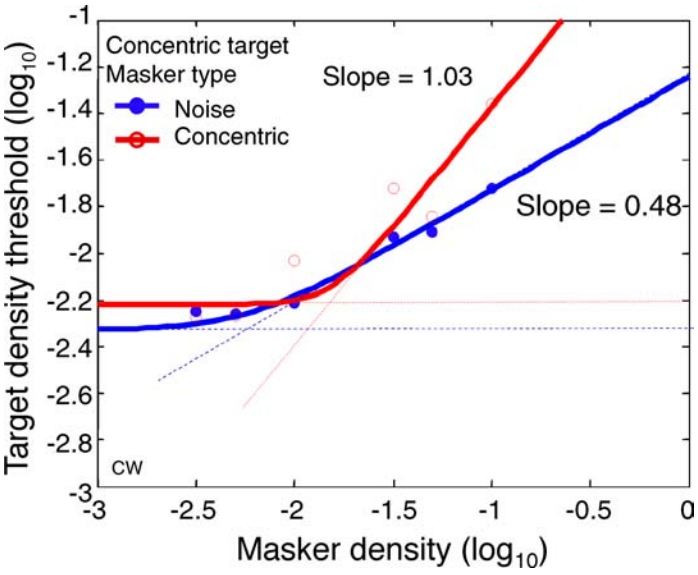

Figure 9. The slope of TvD functions changes with the masker condition. The data shown here are from observer CW as in Figure 3. To better characterize the slope, we considered the TvD function as a fourth power Minkowsky summation of two lines: one horizontal line for the low masker density and one tilted line for the high density. The raising part of the noise masker TvD function (blue closed circles and solid curve) has a slope 0.48. However, for the concentric masker (red open circles and solid curves), the slopes is 1.03.

For the same concentric target, the slope of the TvD function for the noise masker and the concentric masker can differ more than twofold. Hence, the generality of this simple signal-to-noise ratio analysis is limited. A model that takes the interaction between global form detectors into account is necessary to explain our result.

Conclusion

In this study, we measured the target threshold versus masker dot density function for a concentric Glass pattern target superimposed on different Glass pattern maskers. All maskers produced a masking effect if the masker density was great enough. The magnitude of masking depended on the global structure of the masker. For concentric targets, the concentric and spiral maskers produced a greater masking effect than radial and vertical maskers, while for the radial target, the low-curvature spiral masker produced the greatest masking effect. This suggests a curvature selectivity in the global Glass pattern detector. The target threshold versus masker density (TvD) functions is well fit by a divisive inhibition function. In this model, the response of the global mechanism is the excitation of a linear template by the input image raised by a power and divided by the sum of an inhibition input and a constant.

Acknowledgments

Supported by NSC (Taiwan) 96-2413-H-002-006-MY3 to CCC.

Commercial relationship: none.
Corresponding author: Chien-Chung Chen.
Email: c3chen@ntu.edu.tw.
Address: Department of Psychology, National Taiwan University, Taipei 106, Taiwan.

References

Burr, D., & Ross, J. (2006). The effects of opposite-polarity dipoles on the detection of Glass patterns. *Vision Research, 46,* 1139–1144. [PubMed]

Cardinal, K. S., & Kiper, D. C. (2003). The detection of colored Glass patterns. *Journal of Vision, 3*(3):2, 199–208, http://journalofvision.org/3/3/2/, doi:10.1167/3.3.2. [PubMed] [Article]

Chen, C. C. (2006). Local grouping in glass patterns: Chromatic and luminance tuning [Abstract]. *Journal of Vision, 6*(6):759, 759a, http://journalofvision.org/6/6/759/, doi:10.1167/6.6.759.

Chen, C. C., & Foley, J. M. (2004). Pattern detection: Interactions between oriented and concentric patterns. *Vision Research, 42,* 915–924. [PubMed]

Chen, C. C., Chen, K. B., Tseng, C. H., & Kuo, T. Z. (2009). Constructing a metrics for blur perception with blur discrimination experiments. *SPIE Proceedings, 7242,* 724219-1-724219-9.

Chen, C. C., Foley, J. M., & Brainard, D. H. (2000). Detection of chromoluminance patterns on chromoluminance pedestals I: Threshold measurements. *Vision Research, 40,* 773–778.

Chen, C. C., & Tyler, C. W. (2001). Lateral sensitivity modulation explains the flanker effect in contrast discrimination. *Proceedings of the Royal Society of London B: Biological Sciences, 268,* 509–516. [PubMed] [Article]

Chen, C. C., & Tyler, C. W. (2002). Lateral modulation of contrast discrimination: Flanker orientation effects. *Journal of Vision, 2*(6):8, 520–530, http://journalofvision.org/2/6/8/, doi:10.1167/2.6.8. [PubMed] [Article]

Chen, C. C., & Tyler, C. W. (2008). Excitatory and inhibitory interaction fields of flankers revealed by contrast-masking functions. *Journal of Vision, 8*(4):10, 1–14, http://journalofvision.org/8/4/10/, doi:10.1167/8.4.10. [PubMed] [Article]

Clifford, C. W., & Weston, E. (2005). Aftereffect of adaptation to Glass patterns. *Vision Research, 45,* 1355–1363. [PubMed]

Dakin, S. C. (1997). The detection of structure in glass patterns: Psychophysics and computational models. *Vision Research, 37,* 2227–2246. [PubMed]

Dakin, S. C., & Bex, P. J. (2001). Local and global visual grouping: Tuning for spatial frequency and contrast. *Journal of Vision, 1*(2):4, 99–111, http://journalofvision.org/1/2/4/, doi:10.1167/1.2.4. [PubMed] [Article]

Earle, D. C. (1999). Glass patterns: Grouping by contrast similarity. *Perception, 28,* 1373–82. [PubMed]

Foley, J. M. (1994). Human luminance pattern-vision mechanisms: Masking experiments require a new model. *Journal of the Optical Society of America A, Optics, Image Science, and Vision, 11,* 1710–1719. [PubMed]

Gallant, J. L., Braun, J., & Van Essen, D. C. (1993). Selectivity for polar, hyperbolic, and Cartesian gratings in macaque visual cortex. *Science, 259,* 100–103. [PubMed]

Glass, L. (1969). Moiré effect from random dots. *Nature, 223,* 578–580. [PubMed]

Holmes, D. J., & Meese, T. S. (2004). Grating and plaid masks indicate linear summation in a contrast gain pool. *Journal of Vision, 4*(12):7, 1080–1089, http://journalofvision.org/4/12/7/, doi:10.1167/4.12.7. [PubMed] [Article]

Kontsevich, L. L., & Tyler, C. W. (1999). Bayesian adaptive estimation of psychometric slope and threshold. *Vision Research, 39,* 2729–2737. [PubMed]

Kurki, I., & Laurinen, P., Peromaa, T., & Saarinen, J. (2003). Spatial integration in Glass patterns. *Perception, 32,* 1211–1220. [PubMed]

Legge, G. E., & Foley, J. M. (1980). Contrast masking in human vision. *Journal of the Optical Society of America, 70,* 1458–1470.

Legge, G. E., Kersten, D., & Burgess, A. E. (1987). Contrast discrimination in noise. *Journal of the Optical Society of America A, Optics and Image Science, 4,* 391–404. [PubMed]

Lu, Z. L., & Dosher, B. A. (1998). External noise distinguishes attention mechanisms. *Vision Research, 38,* 1183–1198. [PubMed]

Lu, Z.-L., & Dosher, B. A. (2008). Characterizing observers using external noise and observer models: Assessing internal representations with external noise. *Psychological Review,* 115, 44–82. [PubMed]

Maloney, R. K., Mitchison, G. J., & Barlow, H. B. (1987). Limit to the detection of Glass patterns in the presence of noise. *Journal of the Optical Society of America A, Optics and Image Science, 4,* 2336–2341. [PubMed]

Mandelli, M. J., & Kiper, D. C. (2005). The local and global processing of chromatic Glass patterns. *Journal of Vision, 5*(5):2, 405–416, http://journalofvision.org/5/5/2/, doi:10.1167/5.5.2. [PubMed] [Article]

Nachmias, J., & Sansbury, R. V. (1974). Grating contrast: Discrimination may be better than detection. *Vision Research, 14,* 1039–1042. [PubMed]

Pelli, D. G. (1990). The quantum efficiency of vision. In C. Blakemore (Ed.), *Vision: Coding and efficiency* (pp. 3–24). Cambridge, England: Cambridge University Press.

Ross, J., & Speed, H. D. (1991). Contrast adaptation and contrast masking in human vision. *Proceedings of the Royal Society of London B: Biological Sciences, 246,* 61–69. [PubMed]

Seu, L., & Ferrera, V. P. (2001). Detection thresholds for spiral Glass patterns. *Vision Research, 41,* 3785–3790. [PubMed]

Stevens, K. A. (1981). The information content of texture gradients. *Biological Cybernetics, 42,* 95–105. [PubMed]

Stiles, W. S. (1959). Color vision: The approach through increment threshold sensitivity. *Proceedings of the National Academy of Sciences of the United States of America, 45,* 100–114.

Stromeyer, C. F., & Klein, S. (1974). Spatial frequency channels in human vision as asymmetric (edge) mechanisms. *Vision Research, 14,* 1409–1420. [PubMed]

Tyler, C. W., & McBride, B. (1997). The Morphonome image psychophysics software and a calibrator for Macintosh systems. *Spatial Vision, 10,* 479–484. [PubMed]

Webb, B. S., Roach, N. W., & Peirce, J. W. (2008). Masking exposes multiple global form mechanisms. *Journal of Vision, 8*(9):16, 1–10, http://journalofvision.org/8/9/16/, doi:10.1167/8.9.16. [PubMed] [Article]

Wilson, H. R., McFarlane, D. K., & Philips, G. C. (1983). Spatial frequency tuning of orientation selectivity units estimated by oblique masking. *Vision Research, 23,* 873–882. [PubMed]

Wilson, H. R., & Wilkinson, F. (1998). Detection of global structure in Glass patterns: Implications for form vision. *Vision Research, 38,* 2933–2947. [PubMed]

Wilson, H. R., Wilkinson, F., & Asaad, W. (1997). Concentric orientation summation in human form vision. *Vision Research, 17,* 2325–2330. [PubMed]

Wilson, J. A., & Switkes, E. (2005). Integration of differing chromaticities in early and midlevel spatial vision. *Journal of the Optical Society of America A, Optics and Image Science, 22,* 2169–2181. [PubMed]

Wilson, J. A., Switkes, E., & De Valois, R. L. (2004). Glass pattern studies of local and global processing of contrast variations. *Vision Research, 44,* 2629–2641. [PubMed]